nature structural & molecular biology

Structural determinants of miRNAs for RISC loading and slicer-independent unwinding

Tomoko Kawamata[1,2], Hervé Seitz[3,4] & Yukihide Tomari[1,2,5]

MicroRNAs (miRNAs) regulate expression of their target mRNAs through the RNA-induced silencing complex (RISC), which contains an Argonaute (Ago) family protein as a core component. In *Drosophila melanogaster*, miRNAs are generally sorted into Ago1-containing RISC (Ago1-RISC). We established a native gel system that can biochemically dissect the Ago1-RISC assembly pathway. We found that miRNA-miRNA* duplexes are loaded into Ago1 as double-stranded RNAs in an ATP-dependent fashion. In contrast, unexpectedly, unwinding of miRNA-miRNA* duplexes is a passive process that does not require ATP or slicer activity of Ago1. Central mismatches direct miRNA-miRNA* duplexes into pre-Ago1-RISC, whereas mismatches in the seed or guide strand positions 12–15 promote conversion of pre-Ago1-RISC into mature Ago1-RISC. Our findings show that unwinding of miRNAs is a precise mirror-image process of target recognition, and both processes reflect the unique geometry of RNAs in Ago proteins.

At the core of RISCs are Ago family proteins[1–3]. Each small RNA species often binds to a specific Ago protein. In *Drosophila*, miRNAs and siRNAs are actively sorted into Ago1 and Ago2 complexes, respectively[4–6]. The position of mismatches is a key determinant for this small-RNA partitioning. Typical miRNAs, which usually have mismatches in the central region of their miRNA-miRNA* duplexes, are primarily loaded into Ago1, whereas highly complementary exogenous and endogenous siRNAs primarily bind Ago2 (refs. 4–8). A small-RNA sorting system may exist in mammals, although it seems to be less stringent than those in other animals or plants[9,10]. The association of a small RNA with a specific Ago protein dictates its function. Of the four mammalian Ago-subfamily proteins (Ago1–4), only Ago2 possesses target cleavage ('slicer') activity[11,12]. In flies, both Ago1 and Ago2 have slicer activity; however, Ago1 is a much weaker endonuclease than is Ago2 (ref. 5).

RISC assembly follows an ordered, complex pathway[2]. In flies, the RISC-loading complex, which contains Dicer-2 (Dcr-2) and R2D2, has an essential role in loading small RNA duplexes into Ago2-RISC[13–15]. Dcr-2–R2D2 also acts as a gatekeeper in the Ago2 pathway, incorporating siRNA-like perfectly complementary small RNA duplexes and excluding miRNA-like small RNA duplexes[6]. In contrast, how the Ago1-RISC is assembled remains largely unknown. Dicer-1 (Dcr-1) and its partner protein Loquacious (Loqs)[16,17] might have a role in Ago1-RISC loading, by analogy with the function of Dcr-2–R2D2 in Ago2-RISC assembly. In fact, lysate from *dcr-1* null eggs (but not lysate from $loqs^{KO}$ eggs) lacks Ago1-mediated target cleavage activity[18]. However, *dcr-1* lysate cannot be rescued by recombinant Dcr-1 or Dcr-1–Loqs heterodimer[18], raising the possibility that the defect in the *dcr-1* lysate results indirectly from the wide-ranging developmental abnormalities of *dcr-1* eggs[19]. Regardless of a potential role for Dcr-1 in Ago1-RISC loading, it has been implied that an unidentified independent mechanism, in parallel with Dcr-2–R2D2, favors assembly of miRNA-like duplexes into Ago1-RISC[6].

Both the miRNA-miRNA* duplex and siRNA duplex need to be unwound to act as a single-stranded guide in RISC to recognize their target mRNAs. It was originally proposed that an ATP-dependent helicase ('unwindase') separates the two small RNA strands, and the resulting single-stranded guide is then loaded into Ago proteins[20]. However, it was later shown that *Drosophila* Ago2 (refs. 21–23), as well as human Ago2 (ref. 24), directly receive double-stranded small RNA from the RISC-loading complex. Ago2 then cleaves the passenger strand, thereby liberating the single-stranded guide to form mature Ago2-RISC. However, the cleavage activity of fly Ago1 is very inefficient[5], and mammalian Ago1, Ago3 and Ago4 show no cleavage activity[11,12]. Thus, it remains unknown when (before or after RISC loading) and, more importantly, how the two strands are separated in such 'slicer-independent' RISC assembly pathways.

Here we describe a native gel system that can biochemically dissect the fly Ago1-RISC assembly pathway. We show that miRNA-miRNA* duplexes are loaded into Ago1 as double-stranded RNAs in an ATP-dependent fashion. In contrast, unwinding requires neither ATP nor the slicer activity of Ago1. Moreover, we identified the structural determinants of small RNA duplexes for Ago1-RISC loading and subsequent separation of the two strands. Our data collectively show that slicer-independent unwinding is a precise mirror-image process of target recognition, and both processes reflect the unique geometry of RNAs in Ago proteins.

[1]Institute of Molecular and Cellular Biosciences, The University of Tokyo, Japan. [2]Department of Medical Genome Sciences, The University of Tokyo, Bunkyo-ku, Tokyo, Japan. [3]Université de Toulouse, UPS, Laboratoire de Biologie Moléculaire Eucaryote, Toulouse, France. [4]CNRS, Laboratoire de Biologie Moléculaire Eucaryote, Toulouse, France. [5]PRESTO, Japan Science and Technology Agency, Kawaguchi-shi, Saitama, Japan. Correspondence should be addressed to Y.T. (tomari@iam.u-tokyo.ac.jp).

Received 23 February; accepted 3 June; published online 16 August 2009; doi:10.1038/nsmb.1630

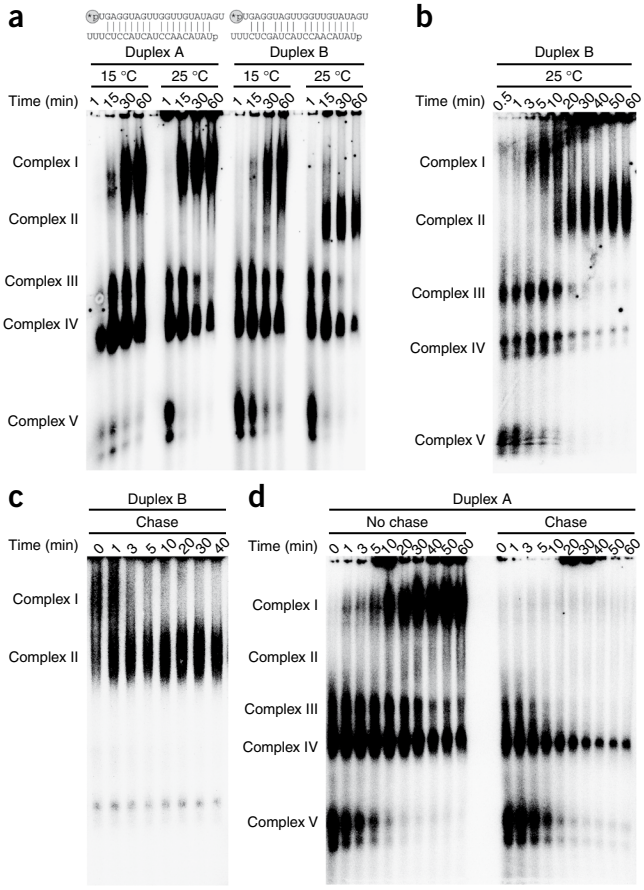

Figure 1 Identification of small RNA–protein complexes in *dcr-2* embryo lysate. (**a**) Native gel analysis in *dcr-2* embryo lysate revealed five complexes (I–V). Lysate and 5′ guide-radiolabeled duplexes were incubated at 15 °C or 25 °C together with nonradiolabeled target mRNA. Complexes assembled at the indicated time points were then separated on a vertical agarose native gel. Structure of duplexes A and B are shown; both duplexes contained the identical guide sequence (above). Asterisk denotes a 5′ ^{32}P group. (**b**) Time course of the complexes formed with duplex B at 25 °C, as in **a**. (**c**) Complex I is a precursor of complex II. Duplex B was incubated with lysate at 15 °C for 60 min, 10-fold excess of nonradiolabeled duplex B was added (time = 0), and 'chase' of complex I into complex II was monitored. (**d**) Complexes III, IV and V are not directly involved in the formation of complexes I and II. Duplex A was preincubated with lysate at 25 °C for 1 min, 10-fold excess of nonradiolabeled duplex A was added (time = 0), and complex formation was monitored.

RESULTS

Intermediate complexes in the Ago1-RISC assembly pathway

To better understand Ago1-RISC assembly, we first sought to biochemically identify complexes formed in the Ago1-RISC assembly pathway. Dcr-2, which is essential for Ago2-RISC loading, is dispensable in the Ago1-RISC assembly pathway[16,17,25]. We therefore used an embryo lysate prepared from *dcr-2*-null mutant flies. We prepared two small RNA duplexes, duplex A and duplex B, which were derived from the natural *let-7*–*let-7** miRNA duplex (**Fig. 1a**). Both duplexes contained an identical guide-strand sequence and a central mismatch at position 10. Duplex B bore an additional mismatch in the passenger strand across from guide position 5 in the seed region, reminiscent of typical miRNA-miRNA* duplexes. We incubated the duplexes radiolabeled with ^{32}P at the 5′ end with lysate at 25 °C, together with a nonradiolabeled ~1,500-nucleotide (nt) target mRNA harboring target sites complementary to the guide strand with a central bulge. We then separated the complexes on a vertical agarose native gel (**Fig. 1a** and **Supplementary Fig. 1**). We detected five distinct ribonucleoprotein complexes, which we tentatively named complexes I–V. For both of the duplexes, complexes III–V appeared almost immediately and then slowly diminished. At later time points (>15 min), duplex A formed only complex I, whereas duplex B formed mostly complex II. At 15 °C, both duplex A and duplex B formed only complex I (**Fig. 1a**).

To determine the relationship between these complexes, we monitored the kinetics of complex formation more intensively. We detected complex I even with duplex B, at very early time points (<10 min) at 25 °C (**Fig. 1b**). Complex II began to form as complex I diminished. These observations imply that complex I is a precursor of complex II. To directly test this hypothesis, we performed 'chase' experiments. We first assembled complex I by incubating radiolabeled duplex B in lysate for 60 min at 15 °C. Subsequently, we added a 10-fold excess of nonradiolabeled duplex B to prevent further incorporation of the radiolabeled duplex B into complex I. At the same time, we shifted the temperature to 25 °C and monitored complex formation. Within 5 min, complex I was completely chased into complex II (**Fig. 1c**), indicating that complex I is a precursor of complex II. We next formed complexes III–V by incubating radiolabeled duplex A for only 1 min at 25 °C and then adding a 10-fold excess of nonradiolabeled duplex. Complexes III–V were not chased into complex I or II (**Fig. 1d**), suggesting that complexes III–V are irrelevant to complex I or II. Single-stranded *let-7*, which was previously tested in a native gel system using *Caenorhabditis elegans* lysate[26], formed complex V at the earliest time point but immediately degraded without forming any other complexes (**Supplementary Fig. 1**).

Complexes I and II contain Ago1

To identify the proteins bound to the duplexes, we incubated duplexes A or B at 25 °C and photo–cross-linked the reaction mixture with 254-nm UV light. We separated each complex on a native agarose gel, excised it from the gel, and analyzed the proteins covalently linked to the radiolabeled duplexes by SDS-PAGE (**Fig. 2a**,**b**). We detected only a ~110-kDa protein in complexes I and II (**Fig. 2b**), and we specifically immunoprecipitated this cross-linked band using antibody to Ago1 (ref. 6; data not shown). Moreover, in a *dcr-2* lysate where ~99% of endogenous Ago1 was immunodepleted, complexes I and II were barely detectable, confirming that complexes I and II contain Ago1 (**Fig. 2c**). We also observed ~250-kDa and ~80-kDa proteins in complex IV (**Fig. 2b**), which we did not attempt to identify because complex IV is not involved in the assembly of the Ago1-containing complexes (**Fig. 1d**).

Complexes I and II are pre- and mature Ago1-RISC, respectively

As both complexes I and II contain Ago1, we hypothesized that complex I represents pre-Ago1-RISC, which contains double-stranded small RNA, and that complex II represents mature Ago1-RISC, which contains single-stranded small RNA. Supporting this hypothesis, when we radiolabeled the passenger strand instead of the guide strand, we detected complex I but not complex II (**Supplementary Fig. 2a**). Moreover, when we incubated guide-radiolabeled duplex A or duplex B in lysate, immunoprecipitated Ago1 and analyzed the Ago1-bound small RNAs, we observed that duplex A, which mainly forms complex I, remained essentially double-stranded, whereas duplex B, which mainly forms complex II, became considerably more single-stranded (**Fig. 2d**).

To directly determine whether the complexes contain double-stranded or single-stranded small RNAs, we separated and excised complexes from native agarose gels. We then extracted the complex-bound RNA by deproteinizing each gel slice using proteinase K,

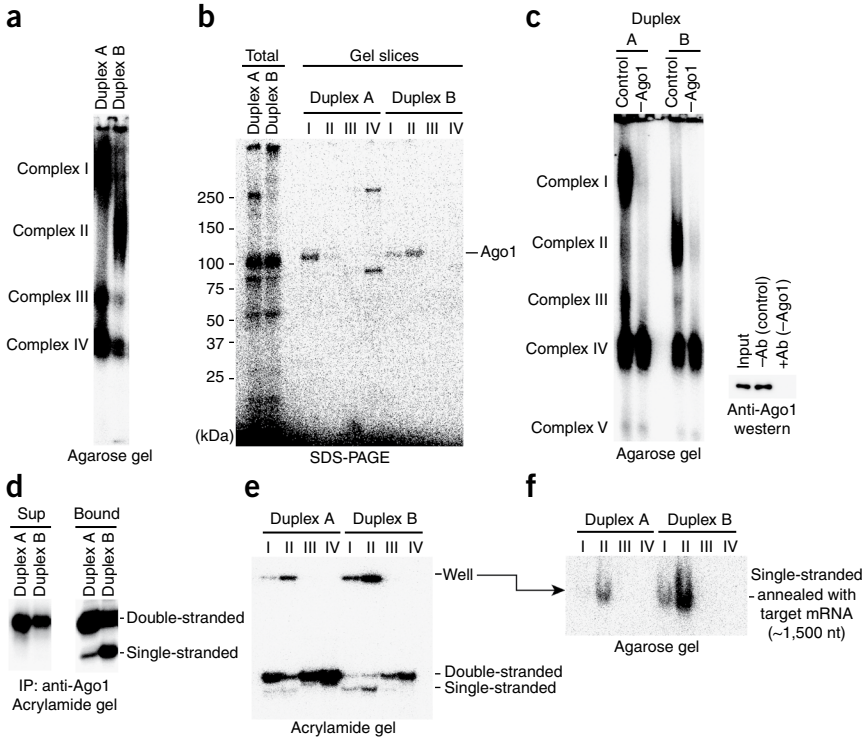

Figure 2 Complex I is pre-Ago1-RISC, and complex II is mature Ago1-RISC. (**a**) Lysate and 5′-radiolabeled duplex A or duplex B were incubated at 25 °C for 30 min as in **Figure 1a**, photo–cross-linked with 254-nm UV light for 5 min and separated on a native agarose gel. (**b**) Each complex (I–IV) was excised from the gel. The proteins photo–cross-linked with duplex A or B were eluted by boiling in SDS loading buffer for 5 min and subjected to 5–20% SDS-PAGE. The ~110-kDa protein detected in complexes I and II was determined to be Ago1. 'Total' indicates photo–cross-linked samples before separation by the native gel. (**c**) Depletion of Ago1 eliminated the formation of complexes I and II. Native gel analysis of the complexes formed in Ago1-immunodepleted, *dcr-2* embryo lysate is shown. Input, supernatant after Ago1 immunodepletion (+Ab) and control (–Ab) are indicated. Efficiency of Ago1 immunodepletion was estimated by western blotting. (**d–f**) Complex I contains double-stranded small RNA, whereas complex II contains single-stranded small RNA. (**d**) Lysate and 5′-radiolabeled duplex A or B were incubated without target mRNA. Ago1 was immunoprecipitated, and Ago1-bound small RNAs were analyzed by 15% polyacrylamide native gel. Sup, supernatant after Ago1 immunoprecipitation; bound, immunoprecipitated Ago1 beads. (**e**) Lysate and 5′-radiolabeled duplex A or B were incubated together with target mRNA for 30 min. Complexes were separated by, and excised from, the native agarose gel, and each of the complex-bound RNAs was extracted and separated by 20% native polyacrylamide gel. (**f**) Samples from **e** were analyzed by 1.4% native agarose gel.

and we separated the RNAs using native polyacrylamide gels. Complex I mostly contained double-stranded small RNA, whereas complex II contained single-stranded small RNA together with another band that barely migrated in the gel (**Fig. 2e**). To analyze this slow-migrating band, we separated the same RNA samples on agarose gels. We detected a band in complex II that corresponded to the single-stranded guide annealed to the target mRNA (**Fig. 2f**). Target RNAs of various lengths affected the mobility of complex II but not that of complex I (**Supplementary Fig. 2b**), suggesting that only complex II can recognize the target RNA. We concluded that complex I is pre-Ago1-RISC, and complex II is mature Ago1-RISC.

Dcr-1 and GW182 are dispensable for Ago1-RISC assembly

Dcr-1, which processes pre-miRNA into the miRNA-miRNA* duplex[25], and GW182, a P-body component required for miRNA-directed translational repression[27,28], are known to associate with Ago1. We assessed whether these proteins are required for Ago1-RISC assembly. We depleted >95% of endogenous Dcr-1 or GW182 in S2 cells by RNA interference (**Supplementary Fig. 3a**). Dcr-1 knockdown abolished pre-miRNA processing activity (**Supplementary Fig. 3b**), and GW182 knockdown markedly impaired Ago1-mediated translational repression (**Supplementary Fig. 3c**). However, depletion of Dcr-1 or GW182 did not affect Ago1-mediated target cleavage (**Supplementary Fig. 3d**) or formation of pre- and mature Ago1-RISC (**Supplementary Fig. 3e**). We concluded that these proteins are dispensable for Ago1-RISC assembly *per se*, although upstream and downstream steps require Dcr-1 and GW182, respectively.

Ago1-RISC loading, but not unwinding, requires ATP

We next determined whether ATP is required for the formation of pre-Ago1-RISC or mature Ago1-RISC. When we depleted endogenous ATP using hexokinase and glucose, we observed neither pre-Ago1-RISC nor mature Ago1-RISC (**Fig. 3a**), indicating that loading of small RNA duplexes into pre-Ago1-RISC requires ATP. Addition of AMP, ADP or nonhydrolyzable ATP analogs did not promote pre-Ago1-RISC formation, indicating that hydrolysis of ATP is essential for Ago1-RISC loading (**Fig. 3b**). We then incubated lysates with radiolabeled duplex B at 15 °C to form pre-Ago1-RISC, depleted ATP at 15 °C, added 20-fold excess nonradiolabeled duplex B and shifted the reaction temperature to 25 °C. Pre-Ago1-RISC was chased into mature Ago1-RISC in the absence of ATP, much as in the presence of ATP (**Fig. 3c**). The identical ATP-depletion protocol at 15 °C completely blocked pre-Ago1-RISC formation of duplex A (**Supplementary Fig. 4**). These observations indicate that formation of pre-Ago1-RISC requires ATP, whereas its conversion into mature Ago1-RISC occurs independent of ATP.

To confirm this, we prepared lysate from S2 cells expressing Flag-tagged Ago1, incubated the lysate with duplex B at 15 °C in the presence of ATP, shifted the temperature to 4 °C to block RISC loading and unwinding, and immunoprecipitated pre-Ago1-RISC using an antibody to Flag. We washed the immunoprecipitate intensively at 4 °C using a high-salt (800 mM NaCl) buffer to remove ATP and most of the Ago1-associated proteins, then monitored unwinding at 25 °C in the presence or absence of ATP. Regardless of the presence of ATP, duplex B in pre-Ago1-RISC was efficiently unwound on the beads, whereas the duplex remained completely double-stranded in lysis buffer only, confirming that ATP is dispensable for unwinding (**Fig. 3d**). These data suggest that Ago1 itself can unwind small RNA duplexes in an ATP-independent fashion, although we cannot exclude the possibility that protein(s) coimmunoprecipitated with Ago1 facilitate unwinding.

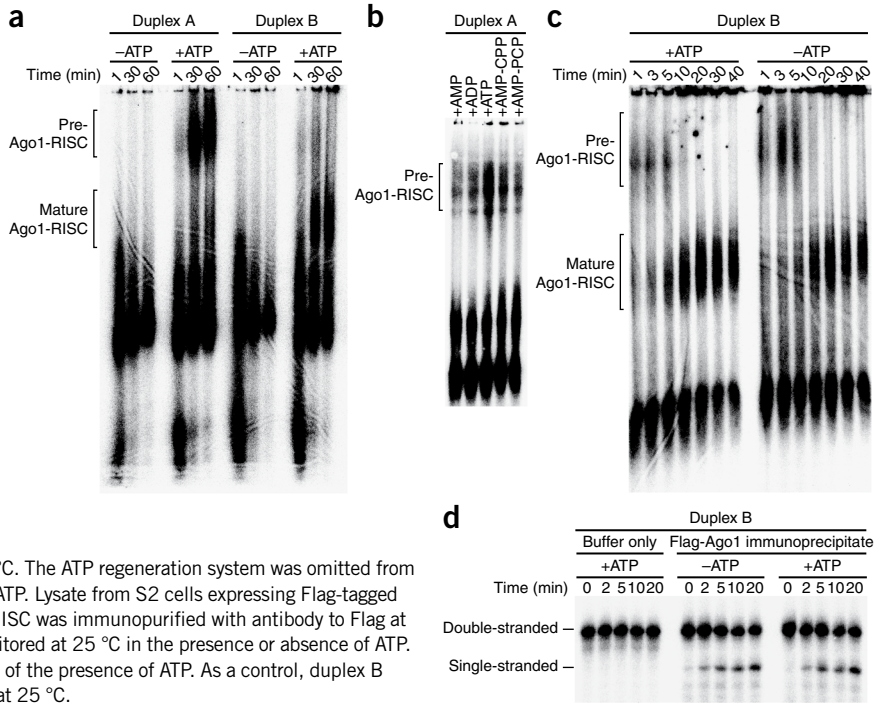

Figure 3 ATP is essential for Ago1-RISC loading but dispensable for unwinding. (**a**) Depletion of ATP blocks small-RNA loading into Ago1. Endogenous ATP was depleted by 0.15 U μl^{-1} hexokinase and 20 mM glucose at 25 °C for 20 min (–ATP, <100 nM ATP). In the mock depletion, no hexokinase was added (+ATP, 1 mM ATP). RISC assembly was done as in **Figure 1a**. (**b**) Hydrolysis of ATP is essential for pre-Ago1-RISC formation. RISC assembly was done using duplex A as in **Figure 1a**, at 25 °C in the presence of 2.5 mM AMP, ADP, ATP, AMP-CPP or AMP-PCP. A basal level of endogenous ATP in *dcr-2* embryo lysate (~10 μM) was present. (**c**) Conversion of pre-Ago1-RISC to mature Ago1-RISC does not require ATP. RISC assembly was done as in **Figure 1a**, at 15 °C for 30 min in the presence of 1 mM ATP to permit pre-Ago1-RISC formation. ATP was depleted from the reaction at 15 °C for 30 min by 0.3 U μl^{-1} hexokinase and 20 mM glucose. A 20-fold excess of nonradiolabeled duplex B was added, the reaction temperature was immediately shifted to 25 °C (time = 0) and complex formation was monitored at 25 °C. The ATP regeneration system was omitted from the assays in **a–c**. (**d**) Unwinding requires Ago1 but not ATP. Lysate from S2 cells expressing Flag-tagged Ago1 was incubated with duplex B at 15 °C, pre-Ago1-RISC was immunopurified with antibody to Flag at 4 °C, and unwinding in the immunoprecipitate was monitored at 25 °C in the presence or absence of ATP. Unwound single-stranded guide was detected regardless of the presence of ATP. As a control, duplex B stayed completely double-stranded in lysis buffer alone at 25 °C.

Central mismatches direct Ago1-RISC loading

As shown above, although both duplexes A and B can enter pre-Ago1-RISC, only duplex B can form mature Ago1-RISC. This prompted us to examine how the structure of duplexes affects pre- and mature Ago1-RISC formation. We prepared 17 small RNA duplexes: a functionally asymmetric *let-7* siRNA duplex, in which the guide and passenger strands were fully paired except at guide position 1 (duplex mm1) and 16 duplex derivatives bearing one additional mismatch at every guide position (duplexes mm2 to mm17; **Supplementary Table 1**). At 15 °C (at which little mature Ago1-RISC is formed), only duplexes mm8 to mm12, peaking at mm10, efficiently formed pre-Ago1-RISC (**Fig. 4a**,**b**), indicating that central mismatches are essential for the formation of pre-Ago1-RISC.

Seed and 3′-mid mismatches promote unwinding

We next prepared another series of 17 duplexes (duplexes MM10/mm1 to MM10/mm17; **Supplementary Table 1**) that were identical to duplexes mm1 to mm17, except that an additional mismatch was introduced at guide position 10 to promote pre-Ago1-RISC formation. At 25 °C, pre-Ago1-RISC containing MM10/mm1 and MM10/mm9 to MM10/mm11 remained largely unconverted, whereas pre-Ago1-RISC containing MM10/mm2 to MM10/mm8 and MM10/mm12 to MM10/mm15 were efficiently converted into mature Ago1-RISC (**Fig. 4c–e**). Thus, seed and 3′-mid (guide positions 12–15) mismatches promote unwinding. We observed that mismatches near the 3′ end of the radiolabeled MM10 strand (MM10/mm16 and MM10/mm17) inverted the strand asymmetry of the small RNA duplexes[29,30] and directed the nonradiolabeled strand into mature Ago1-RISC. A target cleavage assay measuring the amount of mature Ago1-RISC in *dcr-2* lysate confirmed the preference of the seed and 3′-mid mismatches in the (original) mm and MM10/mm series (**Supplementary Fig. 5a**,**b**). Notably, in the mm series, duplexes with a central mismatch (mm9 to mm11) formed more pre-Ago1-RISC (**Fig. 4a**), yet their target cleavage activity was lower than that of duplexes with a mismatch in the seed or 3′-mid regions (**Supplementary Fig. 5a**), which reinforces the requirement of seed or 3′-mid mismatches for Ago1-RISC maturation. Coincidentally, seed matches are not always sufficient for miRNA-mediated gene regulation, and contiguous pairing in the 3′-mid region (positions 12–16) substantially enhances the efficacy[31] (**Fig. 4f**).

Position of mismatches is measured from 5′ end of the guide

Given that the position of a mismatch is crucial to Ago1-RISC loading and maturation, we sought to determine from where the position is measured. To that end, we prepared a series of longer (25-nt) duplexes (**Supplementary Table 1**, 25-nt mm and MM10/mm series) and assayed for Ago1-RISC loading and unwinding. As in the 21-nt duplex series, mismatches at positions 7–11 of the 25-nt duplexes directed the formation of pre-Ago1-RISC (**Supplementary Fig. 6a**,**b**), and mismatches in the seed or 3′-mid regions promoted unwinding (**Supplementary Fig. 6c–e**). Target cleavage assays (**Supplementary Fig. 5c**,**d**) also confirmed these observations. We concluded that the position of mismatch is measured from the 5′ end of the guide, not the 'center' of the duplex or the 3′ end of the guide, for both Ago1-RISC loading and maturation.

G:U wobbles behave like mismatches in Ago1-RISC assembly

G:U wobbles between the seed region of an miRNA and its target mRNA significantly hinder miRNA-mediated translational repression, even though they are as thermodynamically favorable as the A:U base-pair[31–33]. We introduced a G:U wobble at guide positions 5, 9 or 15 of a perfectly complementary duplex (GU5, GU9 or GU15; **Supplementary Table 1**). The G:U wobble in the central region (GU9), but not those in the seed or 3′-mid regions (GU5 or GU15), enhanced Ago1-RISC formation, similar to the mismatch (**Supplementary Fig. 7a**). We then prepared MM10 duplex derivatives containing an A:U base pair, a G:U wobble, or a U:U mismatch at position 5 or 13 (**Supplementary Table 1**). A G:U wobble in the seed or 3′-mid region promoted the conversion of pre-Ago1-RISC into mature Ago1-RISC, similar to a mismatch (**Supplementary Fig. 7b**). These results indicate

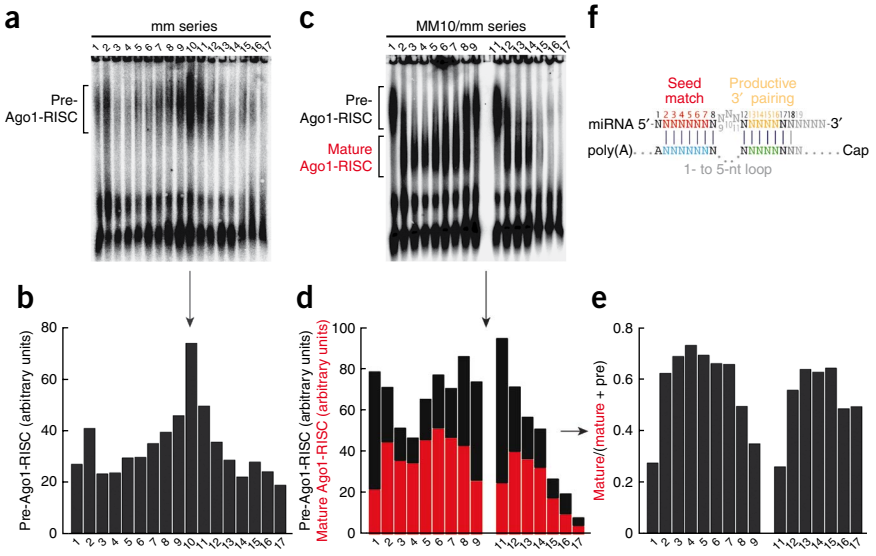

Figure 4 Central mismatches direct small RNA duplexes into pre-Ago1-RISC, whereas seed or 3′-mid mismatches promote conversion of pre-Ago1-RISC to mature Ago1-RISC. (**a**) The 21-nt mm series (mm1 to mm17) was used to assemble pre-Ago1-RISC at 15 °C. (**b**) Quantification of pre-Ago1-RISC in **a**. (**c**) The 21-nt MM10-mm series (MM10-mm1 to MM10-mm17) was used to monitor the conversion from pre-Ago1-RISC to mature Ago1-RISC at 25 °C. (**d**) Quantification of pre-Ago1-RISC and mature Ago1-RISC in **c**. (**e**) Efficiency of strand separation was calculated as (mature Ago1-RISC) / (mature Ago1-RISC + pre-Ago1-RISC). These native gel experiments were repeated five times with excellent reproducibility, and representative data are shown. (**f**) Representation of determinants for efficient target recognition by miRNAs, as reported in ref. 31. Productive 3′ pairing, in addition to seed pairing, promotes efficient target recognition[31]. Preference for mismatches in the seed or 3′-mid regions for Ago1-RISC maturation observed in **c–e** is the reverse of the preference for complete base-pairing in those regions for target recognition by miRNAs.

that G:U wobble base pairs within miRNA duplexes behave similar to mismatches, for both Ago1-RISC loading and unwinding.

Unwinding does not require the slicer activity of Ago1

Ago1 retains slicer activity[4], albeit far less efficient than that of Ago2 (ref. 5). In the Ago2 pathway, cleavage of the passenger strand facilitates the maturation of Ago2-RISC (refs. 21–23). We examined whether the slicer activity of Ago1 is required for Ago1-RISC maturation. Slicer-competent Ago proteins contain the highly conserved Asp-Asp-His (DDH) motif that is required for endonucleolytic activity[11,34,35]. We expressed Flag-tagged Ago1 proteins, in which each residue in the DDH motif was replaced with alanine, in S2 cells. Any mutation in this motif abolished the target cleavage activity of Ago1 (**Fig. 5a**). In contrast, when we immunoprecipitated the tagged Ago1 and separated the Ago1-bound small RNAs on the gel, we detected the same amount of single-stranded guide strand in the mutants as in the wild type (**Fig. 5b**). We then conducted native gel analysis of lysates prepared from cells overexpressing wild-type or mutant Flag-tagged Ago1, in which *dcr-2* was knocked down to eliminate the Ago2 pathway. We detected the same amount of mature Ago1-RISC in the mutants as in the wild type (**Fig. 5c,d**). We concluded that unwinding is independent of the slicer activity of Ago1.

Structures of natural miRNA-miRNA* duplexes

Given the identified structural determinants for Ago1-RISC loading and Ago1-RISC maturation, natural miRNA-miRNA* duplexes should meet such criteria. We used publicly available deep-sequencing datasets of fly miRNAs[36–39], which accurately describe the real miRNA sequences, and predicted the sequences of the miRNA-miRNA* duplexes by 'conceptual dicing' (see Methods). We counted the miRNAs with at least one mismatch in a sliding 3-nt window and observed a significant tendency of mismatches at the

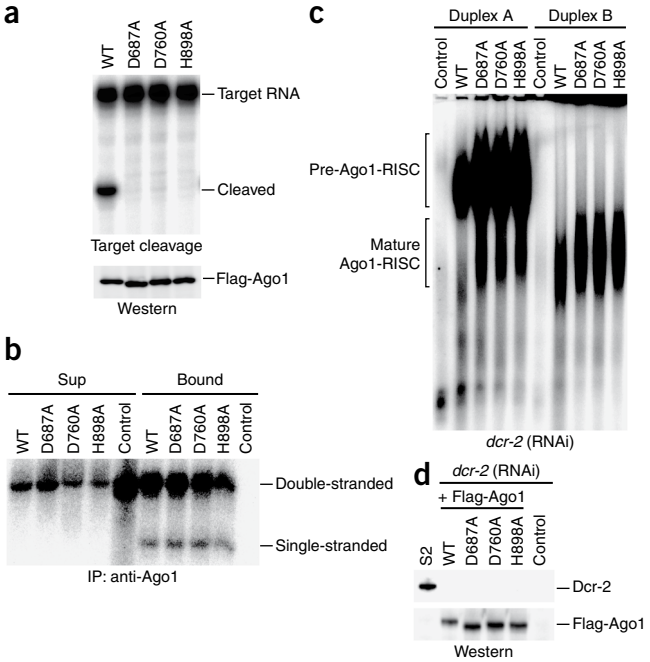

Figure 5 Strand separation of small RNA duplex does not require the slicer activity of Ago1. (**a**) Mutation in the DDH motif abolish target cleavage activity of Ago1. Lysates from S2 cells expressing Flag-tagged wild-type (WT) Ago1 or its mutant derivatives were incubated with nonradiolabeled duplex B. Flag-tagged Ago1 was then immunoprecipitated with antibody to Flag. After extensive washing, target cleavage was monitored. Expression of Flag-tagged Ago1 proteins was confirmed by western blotting (below) using antibody to Flag. (**b**) Mutations in the DDH motif do not affect strand separation of the small RNA duplex. The 5′-radiolabeled duplex B was incubated with lysates from S2 cells expressing Flag-tagged WT Ago1 or its mutant derivatives, and Flag-Ago1 was immunoprecipitated. Ago1-bound RNA was extracted and separated by 20% native polyacrylamide gel. S2 cells that did not express Flag-Ago1 were used as a control. Sup, supernatant after Ago1 immunoprecipitation; bound, immunoprecipitated Ago1-beads. (**c**) Ago1 DDH mutants formed both pre-Ago1-RISC and mature Ago1-RISC. Native gel analysis was done using lysate from S2 cells in which Dcr-2 was knocked down, and WT or mutant Flag-Ago1 proteins were expressed. Lysate from S2 cells in which Dcr-2 was knocked down but no Flag-Ago1 was expressed was used as a control. (**d**) Expression of Flag-tagged Ago1 proteins and Dcr-2 knockdown in lysates used in **c** were confirmed by western blotting.

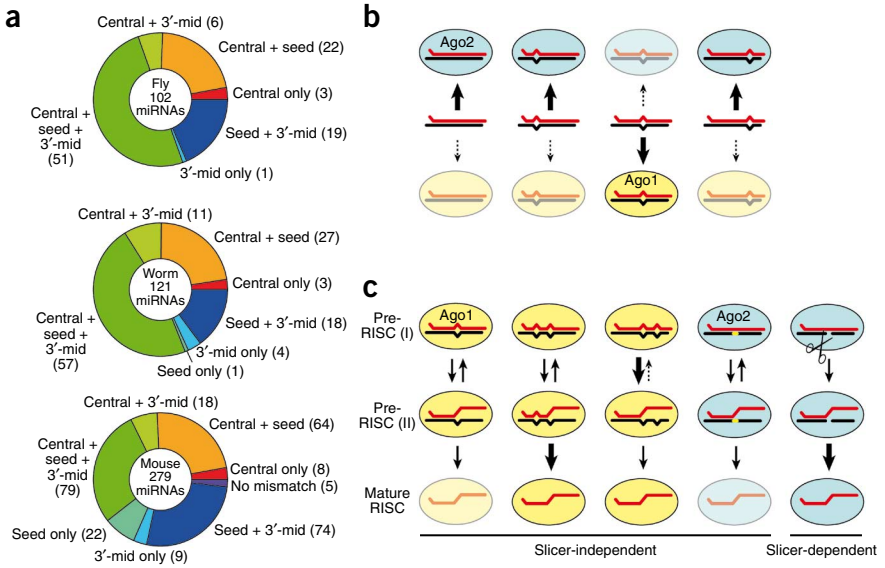

Figure 6 Structural determinants for Ago1-RISC loading and strand separation. (**a**) Structural signature of natural miRNA-miRNA* duplexes in *D. melanogaster*, *C. elegans* and *M. musculus*. Most miRNA-miRNA* duplexes show mismatches in the central region as well as in the seed and/or 3′-mid regions, which ensure efficient RISC loading and unwinding. miRNAs were categorized according to the region(s) where at least one mismatch exists. Seed, guide positions 2–8; central, guide positions 9–11; 3′-mid, guide positions 12–15. (**b**) Efficient Ago1-RISC loading requires central mismatches, which complements the rejection of central mismatches in Ago2-RISC loading[6]. Guide strands are shown in red; passenger strands are shown in black. Solid and dashed arrows indicate strong and weak bindings, respectively. (**c**) Seed and 3′-mid mismatches promote conversion of pre-Ago1-RISC into mature Ago1-RISC, which can be explained by postulating two states of pre-Ago1-RISC: pre-RISC (I), where both the seed and 3′ half regions of the guide can anneal to the passenger, and pre-RISC (II), where the base-pairings are limited to the seed region of the guide (see Discussion). Ago2 usually liberates the guide strand by cleavage of the passenger strand. However, when passenger cleavage is blocked by chemical modification (shown in yellow), a slower 'bypass' mechanism still dissociates the passenger strand[22], which we assume is reminiscent of the slicer-independent unwinding by Ago1. Thick solid, thin solid and dashed arrows indicate fast, moderate and slow reactions, respectively.

5′ end, as well as in positions 9–12 (**Supplementary Fig. 8a**), indicating that natural miRNA-miRNA* duplexes tend to have mismatches in the central region (**Fig. 4a**,**b**). We similarly analyzed miRNA-miRNA* duplexes predicted from *C. elegans*[40,41] and *Mus musculus*[42–45] miRNA deep-sequencing datasets. Whereas worm miRNA-miRNA* duplexes showed a marked frequency of central mismatches (**Supplementary Fig. 8b**), mouse miRNA-miRNA* duplexes showed only a modest central peak (**Supplementary Fig. 8c**), which probably reflects the looseness of small-RNA sorting in mammals[9,10]. We then categorized each miRNA-miRNA* duplex according to the region(s) where at least one mismatch exists (**Fig. 6a**). Of 102 fly miRNAs, 82 (80%) have at least one mismatch in the central region, among which 79 (96%) also have at least one mismatch either in the seed or in the 3′-mid region. Similarly, 81% of worm miRNAs and 61% of mouse miRNAs have at least one mismatch in the central region; among those, 97% and 58%, respectively, also have at least one mismatch either in the seed or the 3′-mid region. Thus, structures of natural miRNA-miRNA* duplexes tend to be optimal for both RISC loading and unwinding.

DISCUSSION

Our data indicate that pre-Ago1-RISC formation requires central mismatches, whereas Ago1-RISC maturation requires mismatches in the seed or 3′-mid regions (**Fig. 4**). Supporting this, our computational analyses show that natural miRNAs tend to have optimal secondary structures of their miRNA-miRNA* duplexes for both RISC loading and maturation (**Fig. 6a** and **Supplementary Fig. 8**). Notably, the preference for central mismatches in Ago1-RISC loading is a perfect complement to the rejection of central mismatches in Ago2-RISC loading[6], thus ensuring accurate sorting of small RNAs in flies (**Fig. 6b**).

Dicer contains a DExD/H-box helicase domain, and genetics and biochemistry have implicated many helicases in the RISC assembly pathway whose functions remain obscure[14,46–51]. Thus, it was plausible that a helicase domain directly unwinds the small RNA duplexes using the energy of ATP when the passenger-strand cleavage pathway is not available. However, our data indicate that unwinding is ATP independent, but the preceding RISC-loading step is ATP dependent (**Fig. 3**). Recent crystal structures of *Thermus thermophilus* Ago protein (TtAgo) bound to DNA guide, or both DNA guide and target RNA, revealed remarkable flexibility of the Ago structure[52,53]. Given that animal Ago proteins are loaded with double-stranded small RNAs from RISC loading machinery, ATP might be used to trigger dynamic conformational opening of Ago proteins to accept RNA duplexes, presumably through interaction between Ago and the RISC loading machinery. We show that at least Dcr-1 and GW182 are dispensable for Ago1-RISC loading (**Supplementary Fig. 3d**,**e**). Further study is warranted to determine the identity of the Ago1-RISC loading machinery.

Our data show that, in contrast to RISC loading, subsequent strand separation does not require the slicer activity of Ago1 or ATP (**Figs. 3** and **5**). Thus slicer-independent unwinding is an unexpectedly passive process. Notably, the preference for mismatches in the seed or 3′-mid regions for Ago1-RISC maturation is the reverse of the previously reported preference for base-pairing in those regions for target recognition by miRNAs[31] (**Fig. 4f**). G:U wobbles are favored for unwinding (**Supplementary Fig. 7b**) and disfavored for target recognition[31–33], both at a level disproportionate to their thermodynamic stability. Both unwinding and target recognition measure the position of mismatches from the 5′ end of the guide[54,55] (**Fig. 4** and **Supplementary Figs. 5** and **6**). Moreover, both unwinding and target recognition and cleavage are, *per se*, ATP independent[27,56] (**Fig. 3c**,**d**). These data indicate that unwinding is a precise mirror-image process of target recognition.

The biased positional effect in base-pairing for unwinding and target recognition might also be explained by the structures of Ago proteins. In the structures of TtAgo, the seed region of the guide strand is preorganized in an A-form helix-like geometry, whereas the 3′ half of the guide strand is disturbed. Although base-pairing in the 3′-half region is dispensable for target cleavage activity of TtAgo[52,53], supplemental base-pairings in 3′-mid regions enhance target recognition in animals[31,56–58]. This contribution of the 3′-mid base-pairings for target recognition can be explained by a so-called

'two-state' model[2,3,59]. In the first state, only the seed region of the guide strand is paired to the target mRNA, whereas the 3′ half of the guide is organized in a way that prevents base-pairing to the target. In the second state, both the seed and 3′ half regions of the guide can anneal to the target mRNA. Because target recognition and cleavage are ATP independent[27,56], we envision that these two states are near-isoenergetic and can rapidly interconvert. Given this model, we reason that pre-RISC also oscillates between the two states—pre-RISC (I), where both the seed and 3′ half regions of the guide can anneal to the passenger, and pre-RISC (II), where only the seed region of the guide is allowed to pair with the passenger (**Fig. 6c**). In these two states, only pre-RISC (II) is favorable for strand separation. In this model, seed mismatches promote conversion of pre-RISC (II) into mature RISC, whereas 3′-mid mismatches shift the equilibrium between pre-RISC (I) and pre-RISC (II) toward pre-RISC (II) (**Fig. 6c**).

Taken together, our analysis of slicer-independent unwinding provides a biochemical explanation for the recognition of target mRNAs by RISC, with both processes being subjected to the identical, unique structural constraints on RNAs by Ago proteins. Because the structural signature of natural miRNA-miRNA* duplexes is conserved among species (**Fig. 6a** and **Supplementary Fig. 8**), our findings for *Drosophila* Ago1 may also explain how non-slicer Ago proteins, such as mammalian Ago1, Ago3 and Ago4, generally separate the two small RNA strands. Moreover, our findings explain why miRNA genes evolutionally retain so many mismatches between their miRNA and miRNA* strands.

METHODS

Methods and any associated references are available in the online version of the paper at http://www.nature.com/nsmb/.

Note: Supplementary information is available on the Nature Structural & Molecular Biology website.

ACKNOWLEDGMENTS

We thank M. Siomi and H. Siomi (Keio University) for the antibody to Ago1, E. Izaurralde (Max Planck Institute) for the antibody to GW182, R. Carthew (Northwestern University) for the *dcr-2*^{L811fsX} flies, and M. Horwich and P. Zamore (University of Massachusetts) for the pENTR-Ago1 construct. We also thank M. Mitomi and A. Maruyama for technical assistance, S. Iwasaki and members of the Tomari laboratory for constant and helpful discussions, and H. Sasaki and P. Zamore for stimulating discussions. This work was supported in part by a Grant-in-Aid for Young Scientists (A) from the Japan Ministry of Education, Culture, Sports, Science and Technology, and a Carrier Development Award from The International Human Frontier Science Program Organization. Y.T. is a Japan Science and Technology Agency PRESTO researcher.

AUTHOR CONTRIBUTIONS

T.K. and Y.T. conducted biochemical experiments, H.S. conducted bioinformatic analyses, Y.T. supervised the study, and all authors discussed the results and wrote the manuscript.

Published online at http://www.nature.com/nsmb/.
Reprints and permissions information is available online at http://npg.nature.com/reprintsandpermissions/.

1. Bartel, D.P. MicroRNAs: genomics, biogenesis, mechanism, and function. *Cell* **116**, 281–297 (2004).
2. Tomari, Y. & Zamore, P.D. Perspective: machines for RNAi. *Genes Dev.* **19**, 517–529 (2005).
3. Filipowicz, W. RNAi: the nuts and bolts of the RISC machine. *Cell* **122**, 17–20 (2005).
4. Okamura, K., Ishizuka, A., Siomi, H. & Siomi, M.C. Distinct roles for Argonaute proteins in small RNA-directed RNA cleavage pathways. *Genes Dev.* **18**, 1655–1666 (2004).
5. Förstemann, K., Horwich, M.D., Wee, L., Tomari, Y. & Zamore, P.D. *Drosophila* microRNAs are sorted into functionally distinct Argonaute complexes after production by Dicer-1. *Cell* **130**, 287–297 (2007).
6. Tomari, Y., Du, T. & Zamore, P.D. Sorting of *Drosophila* small silencing RNAs. *Cell* **130**, 299–308 (2007).
7. Kawamura, Y. *et al.* *Drosophila* endogenous small RNAs bind to Argonaute2 in somatic cells. *Nature* **453**, 793–797 (2008).
8. Ghildiyal, M. *et al.* Endogenous siRNAs derived from transposons and mRNAs in *Drosophila* somatic cells. *Science* **320**, 1077–1081 (2008).
9. Azuma-Mukai, A. *et al.* Characterization of endogenous human Argonautes and their miRNA partners in RNA silencing. *Proc. Natl. Acad. Sci. USA* **105**, 7964–7969 (2008).
10. Su, H., Trombly, M.I., Chen, J. & Wang, X. Essential and overlapping functions for mammalian Argonautes in microRNA silencing. *Genes Dev.* **23**, 304–317 (2009).
11. Liu, J. *et al.* Argonaute2 is the catalytic engine of mammalian RNAi. *Science* **305**, 1437–1441 (2004).
12. Meister, G. *et al.* Human Argonaute2 mediates RNA cleavage targeted by miRNAs and siRNAs. *Mol. Cell* **15**, 185–197 (2004).
13. Liu, Q. *et al.* R2D2, a bridge between the initiation and effector steps of the *Drosophila* RNAi pathway. *Science* **301**, 1921–1925 (2003).
14. Tomari, Y. *et al.* RISC assembly defects in the *Drosophila* RNAi mutant *armitage*. *Cell* **116**, 831–841 (2004).
15. Pham, J.W., Pellino, J.L., Lee, Y.S., Carthew, R.W. & Sontheimer, E.J.A. Dicer-2-dependent 80S complex cleaves targeted mRNAs during RNAi in *Drosophila*. *Cell* **117**, 83–94 (2004).
16. Förstemann, K. *et al.* Normal microRNA maturation and germ-line stem cell maintenance requires Loquacious, a double-stranded RNA-binding domain protein. *PLoS Biol.* **3**, e236 (2005).
17. Saito, K., Ishizuka, A., Siomi, H. & Siomi, M.C. Processing of pre-microRNAs by the Dicer-1-Loquacious complex in *Drosophila* cells. *PLoS Biol.* **3**, e235 (2005).
18. Liu, X. *et al.* Dicer-1, but not Loquacious, is critical for assembly of miRNA-induced silencing complexes. *RNA* **13**, 2324–2329 (2007).
19. Jin, Z. & Xie, T. Dcr-1 maintains *Drosophila* ovarian stem cells. *Curr. Biol.* **17**, 539–544 (2007).
20. Nykänen, A., Haley, B. & Zamore, P.D. ATP requirements and small interfering RNA structure in the RNA interference pathway. *Cell* **107**, 309–321 (2001).
21. Rand, T.A., Petersen, S., Du, F. & Wang, X. Argonaute2 cleaves the anti-guide strand of siRNA during RISC activation. *Cell* **123**, 621–629 (2005).
22. Matranga, C., Tomari, Y., Shin, C., Bartel, D.P. & Zamore, P.D. Passenger-strand cleavage facilitates assembly of siRNA into Ago2-containing RNAi enzyme complexes. *Cell* **123**, 607–620 (2005).
23. Miyoshi, K., Tsukumo, H., Nagami, T., Siomi, H. & Siomi, M.C. Slicer function of *Drosophila* Argonautes and its involvement in RISC formation. *Genes Dev.* **19**, 2837–2848 (2005).
24. Leuschner, P.J., Ameres, S.L., Kueng, S. & Martinez, J. Cleavage of the siRNA passenger strand during RISC assembly in human cells. *EMBO Rep.* **7**, 314–320 (2006).
25. Lee, Y.S. *et al.* Distinct roles for *Drosophila* Dicer-1 and Dicer-2 in the siRNA/miRNA silencing pathways. *Cell* **117**, 69–81 (2004).
26. Chan, S.P., Ramaswamy, G., Choi, E.Y. & Slack, F.J. Identification of specific *let-7* microRNA binding complexes in *Caenorhabditis elegans*. *RNA* **14**, 2104–2114 (2008).
27. Iwasaki, S., Kawamata, T. & Tomari, Y. *Drosophila* Argonaute1 and Argonaute2 employ distinct mechanisms for translational repression. *Mol. Cell* **34**, 58–67 (2009).
28. Eulalio, A., Huntzinger, E. & Izaurralde, E. GW182 interaction with Argonaute is essential for miRNA-mediated translational repression and mRNA decay. *Nat. Struct. Mol. Biol.* **15**, 346–353 (2008).
29. Khvorova, A., Reynolds, A. & Jayasena, S.D. Functional siRNAs and miRNAs exhibit strand bias. *Cell* **115**, 209–216 (2003).
30. Schwarz, D.S. *et al.* Asymmetry in the assembly of the RNAi enzyme complex. *Cell* **115**, 199–208 (2003).
31. Grimson, A. *et al.* microRNA targeting specificity in mammals: determinants beyond seed pairing. *Mol. Cell* **27**, 91–105 (2007).
32. Doench, J.G., Petersen, C.P. & Sharp, P.A. siRNAs can function as miRNAs. *Genes Dev.* **17**, 438–442 (2003).
33. Lewis, B.P., Burge, C.B. & Bartel, D.P. Conserved seed pairing, often flanked by adenosines, indicates that thousands of human genes are microRNA targets. *Cell* **120**, 15–20 (2005).
34. Song, J.J., Smith, S.K., Hannon, G.J. & Joshua-Tor, L. Crystal structure of Argonaute and its implications for RISC slicer activity. *Science* **305**, 1434–1437 (2004).
35. Rivas, F.V. *et al.* Purified Argonaute2 and an siRNA form recombinant human RISC. *Nat. Struct. Mol. Biol.* **12**, 340–349 (2005).
36. Ruby, J.G. *et al.* Evolution, biogenesis, expression, and target predictions of a substantially expanded set of *Drosophila* microRNAs. *Genome Res.* **17**, 1850–1864 (2007).
37. Seitz, H., Ghildiyal, M. & Zamore, P.D. Argonaute loading improves the 5′ precision of both microRNAs and their miRNA* strands in flies. *Curr. Biol.* **18**, 147–151 (2008).
38. Lu, J. *et al.* The birth and death of microRNA genes in *Drosophila*. *Nat. Genet.* **40**, 351–355 (2008).
39. Chung, W.J., Okamura, K., Martin, R. & Lai, E.C. Endogenous RNA Interference provides a somatic defense against *Drosophila* transposons. *Curr. Biol.* **18**, 795–802 (2008).

40. Ruby, J.G. *et al.* Large-scale sequencing reveals 21U-RNAs and additional microRNAs and endogenous siRNAs in *C. elegans*. *Cell* **127**, 1193–1207 (2006).
41. Batista, P.J. *et al.* PRG-1 and 21U-RNAs interact to form the piRNA complex required for fertility in *C. elegans*. *Mol. Cell* **31**, 67–78 (2008).
42. Calabrese, J.M., Seila, A.C., Yeo, G.W. & Sharp, P.A. RNA sequence analysis defines Dicer's role in mouse embryonic stem cells. *Proc. Natl. Acad. Sci. USA* **104**, 18097–18102 (2007).
43. Tam, O.H. *et al.* Pseudogene-derived small interfering RNAs regulate gene expression in mouse oocytes. *Nature* **453**, 534–538 (2008).
44. Baek, D. *et al.* The impact of microRNAs on protein output. *Nature* **455**, 64–71 (2008).
45. Babiarz, J.E., Ruby, J.G., Wang, Y., Bartel, D.P. & Blelloch, R. Mouse ES cells express endogenous shRNAs, siRNAs, and other Microprocessor-independent, Dicer-dependent small RNAs. *Genes Dev.* **22**, 2773–2785 (2008).
46. Ishizuka, A., Siomi, M.C. & Siomi, H. A *Drosophila* fragile X protein interacts with components of RNAi and ribosomal proteins. *Genes Dev.* **16**, 2497–2508 (2002).
47. Robb, G.B. & Rana, T.M. RNA helicase A interacts with RISC in human cells and functions in RISC loading. *Mol. Cell* **26**, 523–537 (2007).
48. Meister, G. *et al.* Identification of novel Argonaute-associated proteins. *Curr. Biol.* **15**, 2149–2155 (2005).
49. Höck, J. *et al.* Proteomic and functional analysis of Argonaute-containing mRNA-protein complexes in human cells. *EMBO Rep.* **8**, 1052–1060 (2007).
50. Landthaler, M. *et al.* Molecular characterization of human Argonaute-containing ribonucleoprotein complexes and their bound target mRNAs. *RNA* **14**, 2580–2596 (2008).
51. Zhou, R. *et al.* Comparative analysis of Argonaute-dependent small RNA pathways in *Drosophila*. *Mol. Cell* **32**, 592–599 (2008).
52. Wang, Y., Sheng, G., Juranek, S., Tuschl, T. & Patel, D.J. Structure of the guide-strand-containing Argonaute silencing complex. *Nature* **456**, 209–213 (2008).
53. Wang, Y. *et al.* Structure of an Argonaute silencing complex with a seed-containing guide DNA and target RNA duplex. *Nature* **456**, 921–926 (2008).
54. Elbashir, S.M., Martinez, J., Patkaniowska, A., Lendeckel, W. & Tuschl, T. Functional anatomy of siRNAs for mediating efficient RNAi in *Drosophila melanogaster* embryo lysate. *EMBO J.* **20**, 6877–6888 (2001).
55. Elbashir, S.M., Lendeckel, W. & Tuschl, T. RNA interference is mediated by 21- and 22-nucleotide RNAs. *Genes Dev.* **15**, 188–200 (2001).
56. Haley, B. & Zamore, P.D. Kinetic analysis of the RNAi enzyme complex. *Nat. Struct. Mol. Biol.* **11**, 599–606 (2004).
57. Doench, J.G. & Sharp, P.A. Specificity of microRNA target selection in translational repression. *Genes Dev.* **18**, 504–511 (2004).
58. Brennecke, J., Stark, A., Russell, R.B. & Cohen, S.M. Principles of microRNA-target recognition. *PLoS Biol.* **3**, e85 (2005).
59. Mallory, A.C. *et al.* microRNA control of PHABULOSA in leaf development: importance of pairing to the microRNA 5′ region. *EMBO J.* **23**, 3356–3364 (2004).

ONLINE METHODS

General methods. Preparation of *Drosophila melanogaster* overnight embryo or S2 cell lysates by Dounce homogenization, 40× reaction mix (containing ATP, ATP regeneration system and RNase inhibitor), and lysis buffer (30 mM HEPES (pH 7.4), 100 mM KOAc and 2 mM $Mg(OAc)_2$) has been described in detail[60]. The *in vitro* RISC assembly assay typically contained 5 µl of lysate, 3 µl of 40× reaction mix, 1 µl of small RNA duplex and 1 µl of target RNA in a total of 10 µl. The *in vitro* target cleavage assay was done with 50 nM small RNA duplex and 1 nM target RNA cap-radiolabeled with ^{32}P. The unwinding assay using 20% native acrylamide gels[6,20], S2 cell culture and knockdown[5], small-RNA radiolabeling with T4 polynucleotide kinase (Takara)[20,60], 254-nm UV cross-linking[6], cap-labeling of target mRNA with guanylyltransferase (Epicentre or Ambion)[6,60] and *in vitro* analysis of Ago1-mediated translational repression[27] were done as described previously.

Preparation of the target mRNAs. A DNA fragment containing the gene encoding *Renilla* luciferase (RL) and four *let-7* target sites in its 3′ untranslated region was amplified by PCR from psiCHECK2-*let-7* 4× (ref. 27). Each target site contained a central bulge to prevent endonucleolytic cleavage by Ago1-RISC. RL 4× mRNA was transcribed using an mScript mRNA production system (Epicentre). We confirmed that mature RISC could be detected using RL 1× mRNA (which contains only one *let-7* target site) with efficiency equal to that of RL 4× mRNA. For the experiments in **Supplementary Figure 2a**, RL 1× mm1 mRNA (which has one target site complementary to the mm1 passenger strand with a central bulge) and RL 1× mm5 mRNA (which has one target site complementary to the mm5 passenger strand with a central bulge) were used. For the experiment in **Supplementary Figure 7b** (left), RL 1× MM10/(U:G)5 mRNA (which has one target site complementary to the MM10/(U:G)5 guide strand with a central bulge) was used.

Native gel analysis. Native gels 1.5–2 mm thick, containing 1.4% (w/v) agarose (Low Range Ultra Agarose, Bio-Rad Laboratories), were cast vertically between glass plates with 0.5-mm-thick bottom spacers (16 cm × 16 cm). To detect intermediate complexes in the Ago1-RISC assembly pathway, 10–20 nM of ^{32}P-radiolabeled duplex and 10 nM of a nonradiolabeled ~1,500-nt target mRNA were incubated under standard RISC assembly assay conditions (see above) at 25 °C or 15 °C. After incubation, the samples were separated by vertical native agarose gel electrophoresis at 300 V for 1.5 h in ice-cold 0.5× Tris-borate-EDTA buffer. Complexes were detected by PhosphorImager (BAS-1500 or FLA-7000 image analyzer, Fujifilm) and quantified using Multi Gauge software (Fujifilm).

Detection of RNA in the complexes. ^{32}P-radiolabeled duplex A or duplex B was incubated with lysate and RL 4× mRNA for 30 min and separated by native gel electrophoresis, after which the complexes were excised from the gel. The gel slices were deproteinized using 1 mg ml^{-1} proteinase K in 2× PK buffer (200 mM Tris (pH 7.5), 300 mM NaCl and 2% (w/v) SDS) at room temperature for 18 h. The eluted RNA was precipitated with ice-cold ethanol and then dissolved in native loading dye and analyzed by electrophoresis.

ATP depletion. ATP was depleted by preincubating lysate with 20 mM glucose and 0.15 or 0.3 U $µl^{-1}$ hexokinase (Sigma) for 30 min at 25 °C (**Fig. 3a**) or 15 °C (**Fig. 3c**). More than 99% of endogenous ATP was depleted (final <100 nM), as measured by ENLITEN luciferase/luciferin reagent (Promega). The ATP regeneration system (creatine kinase and creatine monophosphate) was omitted in the experiments in **Figure 3** and **Supplementary Figure 4**.

Plasmid construction. pENTR-Ago1 was a kind gift from M. Horwich and P. Zamore. Mutations in the *ago1* gene (D687A, D760A, or H898A) were introduced using the QuikChange site-directed mutagenesis kit (Stratagene) to generate the 'entry' clones. The entry clones were recombined with the pAFW destination vector (*Drosophila* Gateway vector collection, Actin5C promoter and N-terminal 3× Flag-tag) using Gateway LR Clonase enzyme mix (Invitrogen).

Transfection. S2 cells (1×10^6 cells ml^{-1}) were transfected with 10 µg pAFW-Ago1 vectors (or their mutant derivatives) per 10 ml culture using FuGENE HD transfection reagent (Roche).

Immunoprecipitation and immunodepletion. Immunoprecipitation was done as previously described[6,27]. The immune complexes were washed three times with lysis buffer containing 0.1% (v/v) Triton X-100 and washed again with 1× lysis buffer. In the experiment in **Figure 3d**, 800 mM NaCl was supplemented in the wash buffer. Ago1 immunodepletion was carried out as described previously[6].

Western blotting. Antibodies to Flag (1:5,000; Sigma), Ago1 (1:10,000; ref. 23), GW182 (1:1,000; ref. 28), Dcr-1 (1:1,000; ref. 16) and Dcr-2 (1:5,000; ab4732, Abcam) were used as the primary antibodies. Chemiluminescence was induced by SuperSignal West Dura substrate (Pierce), and images were acquired by a LAS-3000 imaging system and quantified using Multi Gauge software (Fujifilm Life Sciences).

***In silico* conceptual dicing.** Pre-miRNA sequences were downloaded from miRBase (version 12.0), then extended by 20 nt at each extremity based on the current genome assemblies (April 2006 release of the *D. melanogaster* genome, July 2007 release of the *M. musculus* genome and May 2008 release of the *C. elegans* genome). Pre-miRNA sequences were folded into an unbranched hairpin, using RNAsubopt from the Vienna RNA package (http://www.tbi.univie.ac.at/RNA/) to select the most stable unbranched hairpin within 8 kcal mol^{-1} of the most stable structure. miRNA sequences were extracted from the following GEO data sets: *D. melanogaster*: GSM180329, GSM180330, GSM180332, GSM180333, GSM180335, GSM180336 (ref. 36), GSM239041, GSM239050, GSM239051, GSM239052, GSM239053, GSM239054, GSM239055, GSM239056 (ref. 37), GSM246084 (ref. 38), GSM272651, GSM272652, GSM272653 and GSM275691 (ref. 39); *M. musculus*: GSM237107, GSM237110 (ref. 42), GSM261957, GSM261959 (ref. 43), GSM304914 (ref. 44), GSM314552 and GSM314558 (ref. 45); *C. elegans*: GSM139137 (ref. 40), GSM297743, GSM297744, GSM297746, GSM297747, GSM297750, GSM297751 and GSM297757 (ref. 41). To include every alternative processing isoform, all of the libraries of a given species were pooled, and up to 9 nt of distance between the observed isoforms and the miRBase-annotated isoform was tolerated. miRNA* sequences were extracted from the folded pre-miRNA hairpins, considering that a miRNA* pairs to the miRNA, with each strand showing a 2-nt 3′-overhang.

Analysis of structural signature of natural miRNA-miRNA* duplexes. miRNAs with at least 100 reads in the pooled deep-sequencing libraries were selected. For each miRNA, the most abundant isoform was selected from the pooled deep-sequencing libraries, and its most stable miRNA-miRNA* duplex structure was predicted using RNAcofold from the Vienna RNA package. For the analyses in **Supplementary Figure 8**, a 3-nt window centered at each position was slid across the miRNA strand (guide positions 2–17). For each window, we then calculated the mean and standard error of the random variable x, defined by $x = 1$ if there is at least one mismatch in the window, and $x = 0$ if there is no mismatch. For the analyses in **Figure 6a**, positions of mismatches in each miRNA-miRNA* duplex were recorded and classified as described in Results.

60. Haley, B., Tang, G. & Zamore, P.D. In vitro analysis of RNA interference in *Drosophila melanogaster*. *Methods* **30**, 330–336 (2003).